East European Journal of Physics. 3. 346-354 (2023)
DOI:10.26565/2312-4334-2023-3-36 ISSN 2312-4334

THE EFFECT OF DOPING ON THE ELECTRICAL CONDUCTIVITY OF VANADIUM OXIDE (V_2O_5) FILMS DOPED WITH NICKEL OXIDE (NiO) PREPARED VIA PULSED LASER DEPOSITION (PLD)†

Sadon Hassan Hamad*, Huda Saadi Ali#
Department of Physics, College of Education for Pure Sciences, Tikrit University, Salahuddin, Iraq
**Corresponding Author e-mail: sadon.h.hamad@st.tu.edu.iq*
#e-mail: huda.wahbi@tu.edu.iq
Received June 3, 2023; revised July 15, 2023; accepted August 5, 2023

In this research, the focus was on examining thin films of vanadium oxide (abbreviated as V_2O_5) with different levels of doping using nickel oxide (NiO) (X = 0, 6, 8)%. The films were created through pulsed laser deposition (PLD) method. The thin films were made and subjected to annealing at 450°C for a duration of one hour. The structural properties of the films were examined using the XRD diffraction technique, whereby the films' composition was found to be polycrystalline, featuring an orthorhombic structure. Notably, the films displayed a prominent alignment along the (111) plane, manifesting at an angle measuring approximately 27.889°. The FE-SEM technology was utilized to explore and evaluate the surface morphology of the thin films. This showed a nanotube-to-spherical shape transformation. Following the implementation of EDX x-ray technique, it was determined that the films comprised the elemental components of vanadium (V), nickel (Ni), and oxygen (O), consistent with the doping ratios. The assessment of the films' optical properties was carried out through the utilization of UV–visible spectrophotometer, demonstrating decreased absorbance and absorption coefficient, as well as an increased energy gap from 2.32 eV to 2.93 eV. The electrical conductivity results indicated a decrease in direct current conductivity ($\sigma_{d.c}$) with increasing doping ratio, while the activation energy (E_a) increased. Consequently, these films can be utilized in thermoelectric generators.
Keywords: *Thin films; Vanadium oxide (V_2O_5); Pulsed laser deposition (PLD); Annealing; Electrical properties*
PACS: 68.55.-a, 73.25.+I, 74.62.Dh, 78.20.Ci.

1. INTRODUCTION

The technological advancement in various fields such as electro-optics, magnetism, and optics heavily relies on the thin film technology. The fundamental characteristics of thin films encompass their crystalline structure, membrane thickness, and other distinctive properties not present in bulk materials. The composition of thin films primarily depends on the preparation technique and can exist in the form of random polycrystalline or single-crystal membranes. Furthermore, the electrical and optical properties of the films exhibit variations. This is in view of two pieces of evidence. Firstly, the crystalline structure in addition to the presence or absence of impurities. In general, thin films belong to the solid-state category, allowing for their classification based on their crystalline composition or atomic arrangement. Researchers have employed diverse deposition techniques including spray deposition [1], electron beam evaporation [2], sol-gel [3], thermal evaporation [4], pulsed laser deposition (PLD) [5], and so forth.

Vanadium pentoxide, chemically represented as V_2O_5, is an inorganic compound commonly known as vanadium oxide. It is a solid material with a yellowish crystalline structure, and when precipitated from an aqueous solution, it appears dark orange [1,6]. The pentavalent state of vanadium in Vanadium pentoxide stands out as the most stable oxide showing the ultimate level of oxidation compared to other oxides. The lattice parameters of vanadium pentoxide are as follows: a = 11.516 Å (length along the "a" axis), b = 3.565 Å (length along the "b" axis), and c = 4.372 Å (length along the "c" axis). These parameters determine the dimensions of the crystal structure [7,8]. The layered structure of V_2O_5 consists of chains of shared square pyramids (VO_5) at the edges, linking these chains together through corner sharing. Vanadium pentoxide is considered a n-type semiconductor material with multiple valence states, displaying wide energy bandgap transitions that span two values starting from 2.2 eV reaching 2.3 eV [9,10]. With its transformation into a thin film, the material experiences fluctuations in its electrical properties, rendering it an effective catalyst because of its interconnected electrical and optical characteristics. Consequently, it holds promising prospects for diverse applications across multiple domains [11,12], such as microelectronics, optoelectronic devices, solar cells, electrical appliances, electronic switches, and optics, among others [13].

Nickel (II) oxide, with the chemical formula NiO, is a chemical compound that possesses exceptional physical and chemical properties. It holds significant importance in advanced research disciplines and has emerged as one of the few metal oxides of type P with promising prospects in various applications [14]. NiO has a bandgap ranging from 4.3 eV to 3.6 eV. Distinguished by its inherent chemical stability, minimal toxic levels, remarkable resilience, and elevated ionization potential, the material possesses a valuable assemblage of attributes. Moreover, it can be manufactured at low costs, making it economically viable. Additionally, NiO possesses distinct characteristics such as excellent electrical, optical, and magnetic properties [15]. Functioning as a proficient sensor for gas and exemplifying a prototype for semiconductor materials, it demonstrates its aptitude in both aspects. This can be fabricated using a range of physical and chemical methods [16].

† ***Cite as:*** S.H. Hamad, H.S. Ali, East Eur. J. Phys. 3, 346 (2023), https://doi.org/10.26565/2312-4334-2023-3-36

The investigation of Nio's particular structural characteristics as well as the optical, and electrical ones was carried out utilizing the PLD method in this study.

2. Practical Part

2.1 Preparation of powder substances and discs

High-purity vanadium oxide (V_2O_5) with a purity of (99.0%) was used, prepared by the German company Merck, and high-purity nickel oxide (NiO) with a purity of (99.9%) was prepared by the American company Sky Spring Nanomaterials. The powders were weighed using a sensitive electronic balance (Mettler. A.K-160) with a sensitivity of 10^{-5} gm. After weighing the powders, vanadium oxide (V_2O_5) and nickel oxide (NiO) were mixed in different weight ratios (X=0.6, 8)% to obtain a sample weighing 3g. The physical mixing method was used to achieve high homogeneity between pure vanadium oxide particles and the samples doped with nickel oxide. The powders were ground using a ceramic mortar for half an hour. Subsequently, the mixed powders were compressed with a pressure of 3 tons in a special mound made of stainless steel, measuring 1.5cm in diameter and a thickness of 0.5cm, using an American hydraulic press manufactured by Across International.

2.2- Glass Substrate Preparation

Glass substrates with geometric dimensions of 75mm×25mm×0.2mm were used for thin film deposition. The substrates were of AFCO type and were cleaned prior to the deposition process. The following steps were followed:

- The glass substrates were washed with distilled water to remove dirt and impurities from their surfaces.
- After washing with distilled water, the glass substrates were immersed in a glass container containing 96% ethanol for 20 minutes.
- The glass substrates were dried using a soft cloth and stored in dedicated holders.

2.3- Sedimentation system

The application of a Nd:YAG Laser System was observed in the course of depositing thin films onto glass substrates. The system consists of a computer-controlled power supply, an internal cooling system, and a manually adjustable laser beam path on the target. The laser beam has a wavelength of λ = 1064nm, an energy of 800 mJ, a frequency of 6 Hz, and a pulse duration of 10ns. A precise positioning of the laser beam is achieved as it is directed at a fixed15cm from the target material. This is placed inside a cylindrical quartz chamber with low-pressure air (10^{-3}mbar) at room temperature. The glass slide is positioned 3cm above the target material and is subjected to the laser beam at an incident angle of 45°. A total of 800 pulses are used to obtain the desired thin films. The deposition and growth of thin films are facilitated through the PLD interacting with the target material.

2.4- Annealing

The annealing process is used to improve the properties of thin films, where the surface is subjected to a controlled heating process for a specific duration. The purpose of annealing is to eliminate stresses in the material, facilitate the diffusion and arrangement of impurities, increase electrical efficiency, and minimize structural defects resulting from manufacturing. The prepared thin films were annealed using an electric furnace (MUFFLE FURNACE, model MF-12). The thin films are subjected to a temperature of 450°C for a duration of one hour, after which they undergo natural cooling inside the furnace. This process renders the films ready for the to perform the following checks:

2.4.1- Measuring thickness of films

Measuring the thickness of films was performed utilizing the optical interferometer method. For the experimentation, we employed a helium-neon laser operating at a wavelength of 632 nm. The laser beam was directed towards the film at an inclination of 45 degrees. The reflected beam passed through a converging lens and was projected onto a screen to observe interference fringes, as depicted in (Figure 3).

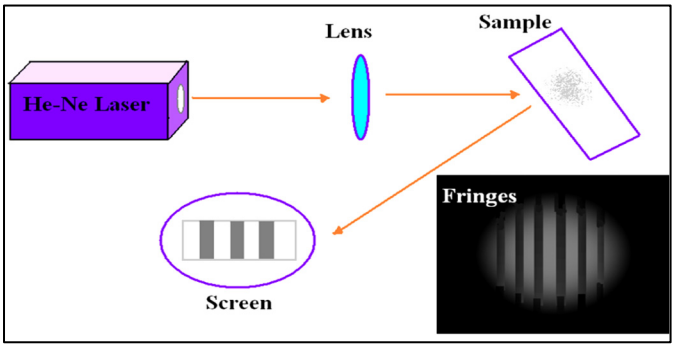

Figure 3. Schema of optical interferometer technique for quantifying the thin films'level of thickness. The fabricated films exhibited an estimated thickness of (500 ± 50)nm.

By measuring the width of the bright fringes (x) and the dark fringes (Δx), The determination of the film thickness can be achieved by applying the following correlation

$$t = \frac{\Delta x}{x} \times \frac{\lambda}{2}. \quad (1)$$

2.4.2- Structural Measurements

To conduct structural evaluations, the films were subjected to XRD using a Shimadzu X-ray machine (model PW1730) produced by Shimadzu in Japan. The XRD instrument employed a wavelength measured at 1.541874 Å [Cd Kα radiation], operated at 40 kV and 30 mA [voltage, current], and encompassing 80˚-10˚ [scanning range]. The calculation of the average grain size (specifically crystallite) of the thin films utilized the Debye-Scherrer relationship.

$$G.S = \frac{K\lambda}{\beta \cos\theta}, \quad (2)$$

where K is a constant parameter with a precise numerical value of 0.94, β corresponds to the peak's width at half of its maximum intensity (FWHM), θ designates the angle of diffraction, indicating the angle at which X-rays are dispersed by the crystal lattice, λ represents the specific wavelength of the X-ray employed for the analysis, specifically Cu Kα with a value of 1.5405 Å. [17,18].

Furthermore, the surface morphology of the membranes was investigated by field-emission scanning electron microscopy FE-SEM and energy dispersive X-ray spectroscopy EDX attached to the FE-SEM device using a (model ZEISS SIGMA VP) device manufactured by Carl Zeiss Microscopy in United States, field emission FE-SEM produces clearer, less electrostatically distorted images with spatial resolution down to 1 1/2 nanometers.

2.4.3- Optical Measurements

A UV-Vis was employed to analyze the optical characteristics of the aforementioned films. The model used was (model 1900) manufactured by SHIMADZU in Japan, located at the College of Pure Science, Department of Physics, Tikrit University. The absorbance spectrum was obtained, and the absorbance range served as the basis for the calculation of the absorbance coefficient of the prepared films. The following formula was adopted [19,20]:

$$\alpha = 2.303 \frac{A}{t}. \quad (3)$$

The absorbance coefficient (α) is a parameter that quantifies the level of light absorption exhibited by a material. The absorbance (A) is a measure of the amount of light that the material absorbs. On the other hand, the film thickness (t) provides valuable information regarding the physical dimensions of the film.

The determination and calculation of the lowest-energy transition value for the thin films were performed for the allowed direct transitions using the following equation

$$\alpha(h\upsilon) = A'(h\upsilon - E_g)^r, \quad (4)$$

Where: E_g – energy gap, α – absorption coefficient, A' – proportionality constant, r – exponential coefficient [21].

2.4.4- Measurements#Electrical

By utilizing a versatile multimeter (Fluke-8846A), the electrical resistance (R) of the thin films was measured across a temperature range, enabling the investigation of their electrical properties. The resistance value of the film ® was recorded for a specific range of temperature variations, with an increment of 10˚C.

The electrical conductivity depends on two main factors: the density level of charge carriers and its mobility as influenced by the electric field. These factors vary with temperature, doping ratios, and preparation conditions. The direct current electrical conductivity (σ_{dc}) is the reciprocal of the specific electrical resistivity (ρ), as shown in the following equation [22]:

$$\boldsymbol{\rho = R\frac{A}{L} \quad where \{ A = b . t \}}, \quad (5)$$

$$\boldsymbol{\sigma_{dc} = \frac{1}{\rho}}, \quad (6)$$

Where:

σ_{dc}: continuous electrical conductivity with units of $(\Omega.cm)^{-1}$, ρ: specific resistivity, R: electrical resistance of the film measured practically in (Ω), L: distance between the aluminum electrodes in (cm), A: cross-sectional area for electron movement through the film, b: electrode width (cm), t: film thickness in nm, converted to (cm)

Semiconductors typically exhibit a negative temperature coefficient of resistance, and their conductivity generally follows an exponential pattern that is influenced by temperature. Consequently, an equation can be formulated to describe the nature of connection that electrical conductivity displays in relation to temperature, enabling the determination of the activation energy. This equation bears resemblance to the well-known Arrhenius equation [23]:

$$\sigma_{dc} = \sigma_o exp\left(\frac{-E_a}{K_B T}\right) \quad .(7)$$

In the present study, the following variables are considered:
E_a: representing the activation energy for electrical conduction measured in eV and corresponding to the difference between Ec and E_F [24], σ_o: denoting the minimum metallic conductivity, T: the absolute temperature in Kelvin, k_B: the Boltzmann constant equal to ($k_B = 1.38\times10^{-23}$ J/K = 0.086×10^{-3} eV/K).

By employing Equation (7), a plot of (ln σ_{dc}) against (1000/T) is generated. The slope of the resulting straight line is equal to ($-E_a/k_B$), allowing for the determination of the activation energy E_a in units of eV [25]:

$$E_a = \text{-slope} \times k_B \times 1000 \quad (8)$$

3- RESULTS AND DISCUSSION

3.1- X-Ray diffraction

The XRD examination performed has revealed that the pure vanadium oxide (V_2O_5) and nickel oxide (NiO) and films of V_2O_5 were doped using varying levels of dopants (X =0.6,8)% possess a crystalline structure of the orthorhombic phase. The diffraction peaks were observed at angles (12.12°, 15.390°, 18.366°, 26.342°, 27.889°, 29.033°, 30.665°,37.305°, 43.348°, 63.017°) corresponding to the planes (101), (002), (100), (011), (111), (301), (220), (200), (111) as depicted in (Figure 4). These findings are in agreement with the International Centre for Diffraction Data (JCPDS Card No: PDF-85-2422), indicating that the (111) plane is the dominant growth direction for both pure and NiO-doped V_2O_5 films. The dominant direction (111), corresponding to the angle (2θ = 27.889°), remained unchanged after doping. Additionally, with an increase in the doping level, there was a corresponding reduction in the how intense the diffraction peaks get, which suggests that doping reduces the grain size of V_2O_5 [26]. In the case of the 8% doping ratio, the grain was measured at 29.293 nm. The grain size of the doped V_2O_5 films exhibited a significant reduction when compared to the grain size of the pure V_2O_5 films. (55.536 nm) as shown in Table 1. These findings are consistent with previous studies [27-29].

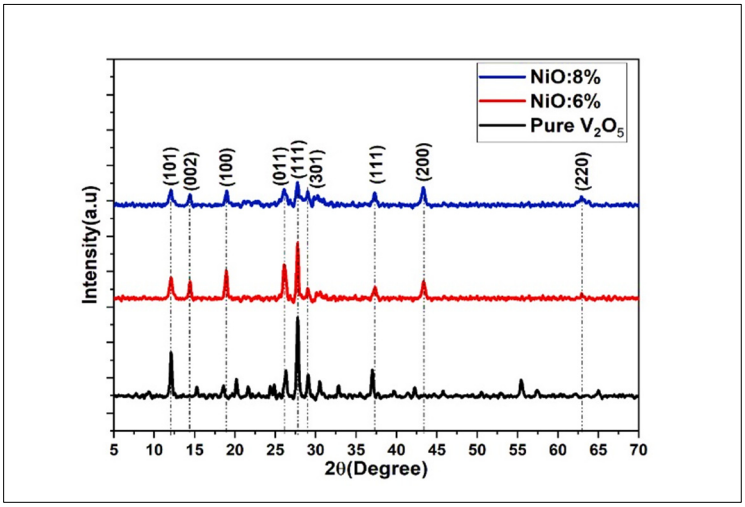

Figure 4. (XRD) patterns of (V_2O_5) films, including both the pure films and the films doped with (NiO)

Table 1. X-ray examination results of pure and Nickel oxide -doped vanadium pentoxide films

Sample	2θ exp (Deg)	2θ std (Deg)	d exp (Å)	d Std (Å)	FWHM	hkl	G.S (nm)
Pure V_2O_5	27.889	27.882	3.195	3.197	0.145	111	55.536
V_2O_5 +NiO(6%)	27.780	27.882	3.208	3.197	0.236	111	34.130
V_2O_5 +NiO(8%)	27.729	27.882	3.213	3.197	0.275	111	29.293

3.2- Field emission scanning electron microscope (FE-SEM)

As can be seen in Figure 5, the assessment of the surface morphological properties of the thin films, specifically focusing on the influence of doping, utilizing (FE-SEM). Images of both (Pure V_2O_5) and (NiO) films were captured using (FE-SEM). Nanoparticles with a nanotube structure and an average size of 89.32 nm were observed in (Figure a).

However, the introduction of doping caused agglomeration as a result of secondary growth on the film surface. This resulted in spherical particles [30,31]. This doping-induced transformation reduced the nanoparticle size to an average range of 37.96 - 24.56 nm in (Figures b, c), while concurrently enhancing surface smoothness through recrystallization. This interesting phenomenon is compatible with various medical applications in the future, including in the field of biomedicine, where vanadium oxide was used because of its strong effect as an inhibitor of blood vessels, as well as in disease resistance and chemotherapy [32].

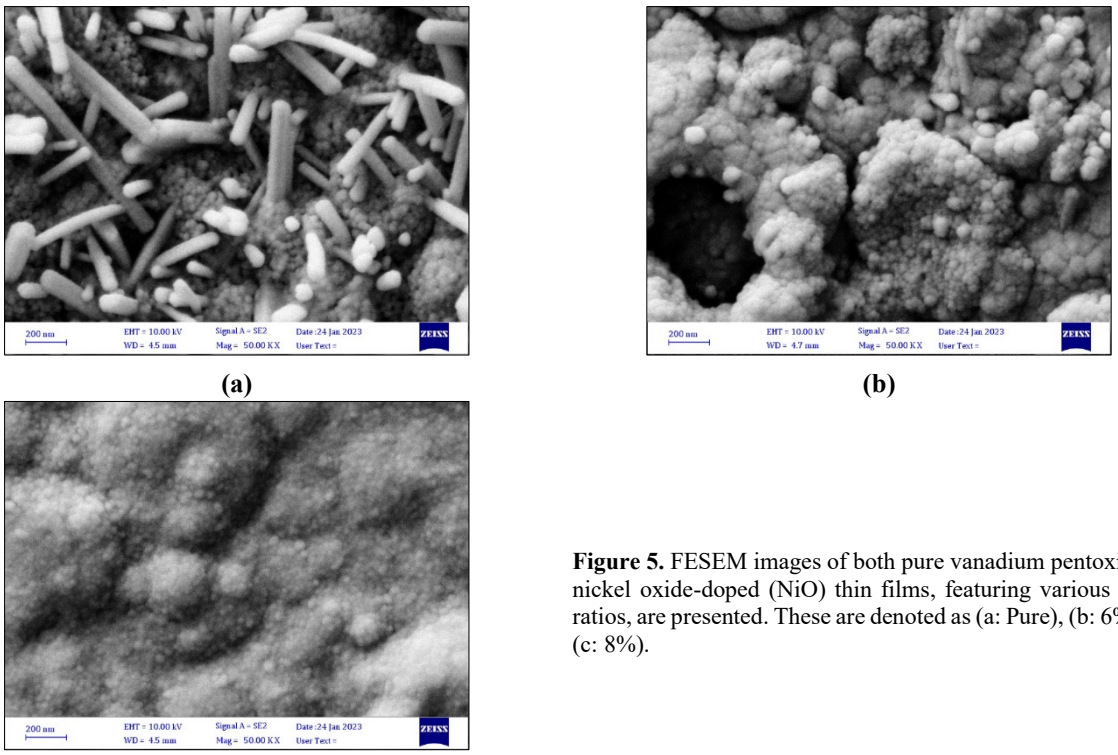

Figure 5. FESEM images of both pure vanadium pentoxide and nickel oxide-doped (NiO) thin films, featuring various doping ratios, are presented. These are denoted as (a: Pure), (b: 6%), and (c: 8%).

3.3- X-ray energy dispersive spectroscopy (EDX)

Figure 6 showcases the EDX results. It can be noted that there are multiple peaks corresponding to different elements in the thin film samples. As regards (Pure: 0%), the noticed peaks indicate the presence of vanadium (V = 90.3 wt%) and oxygen (O = 9.7 wt%), along with gold (Au) from the sample coating used for examination purposes. In the first doping ratio of 6% nickel oxide, the peaks of vanadium (V = 76.2 wt%) and oxygen (O = 8.5 wt%) are observed, along with trace amounts of nickel (Ni = 15.3 wt%), confirming its incorporation as an impurity within the crystal structure of vanadium pentoxide. In the second doping ratio of 8% nickel oxide, the peaks of vanadium (V = 51.3 wt%) and oxygen (O = 5.4 wt%) are detected, along with significant peaks of nickel (Ni = 43.3 wt%). Notably, the peak corresponding to gold, present in the coated films for examination purposes, is not observed. No other elements associated with impurities or contamination were detected, reaffirming the purity of the studied films in this research.

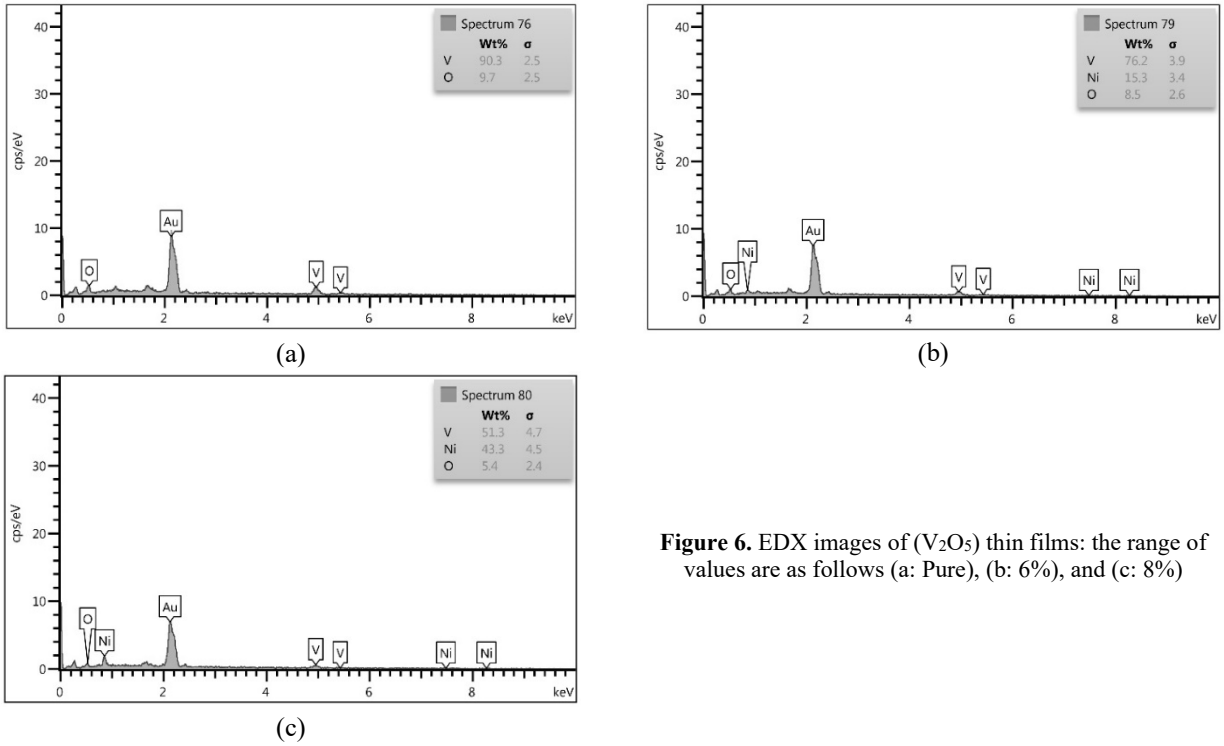

Figure 6. EDX images of (V_2O_5) thin films: the range of values are as follows (a: Pure), (b: 6%), and (c: 8%)

3.4- Optical Properties

3.4.1- Absorbance (A)

The examination of the optical characteristics of the thin films involved analyzing the absorption spectra within the extended wavelength range of 400 nm to 1000 nm. This analysis enabled the determination of the optical constants. It was observed that the absorbance slightly decreases in the high-wavelength region, while A substantial enhancement in absorbance is observed within the area of shorter wavelengths, as shown in (Figure 7). The absorption edge for pure vanadium oxide occurs at 430 nm [33]. Of particular importance is the observation that the absorbance diminishes as the doping ratios increase, primarily as a consequence of a reduction in particle size and an elevation in the optical energy bandgap caused by the presence of nickel oxide (NiO) impurities within the bandgap.

3.4.2- Absorption Coefficient (α)

In a comparable manner to absorbance, the absorption coefficient exhibits a decrease as doping ratios increase, owing to the creation of impurity levels within the energy bandgap, as visually depicted in (Figure 8). At lower levels of photon energy, the absorption coefficient remains minimal, indicating a limited likelihood of electronic transitions. Nevertheless, as the absorption edge is approached towards higher energy levels, the absorption coefficient experiences an increment [34].

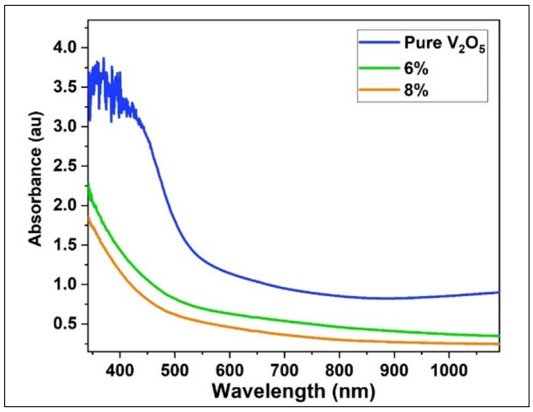

Figure 7. It is clear Absorbance change as a function of wavelength

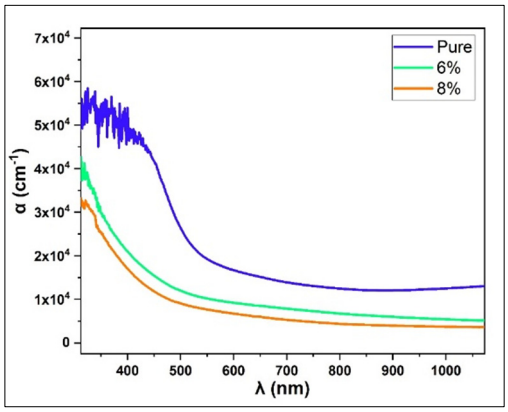

Figure 8. provides a visual representation showcasing the changes in the absorption coefficient as a function of photon energy

3.4.3- The Optical Energy Gap (E_g)

The direct bandgap semiconductors known as V_2O_5 membranes possess an approximate energy gap of 2.3 eV. Upon introducing nickel oxide (NiO) as a dopant, equation (4) was employed to compute the optical energy gap value for permissible direct transitions. The plotted relationship between (αhv)2 and photon energy (hv) is depicted in (Figure 9), highlighting that the optical energy gap exhibits a conspicuous amplification in its magnitude as the doping ratio increases. This augmentation in the value of the energy gap can be ascribed to the emergence of levels within the energy gap caused by NiO, consequently resulting in the narrowing of said levels [35]. In its pure form, vanadium oxide (V_2O_5) exhibits an energy gap of 2.32 eV. However, when doped with nickel oxide at a rate of 6%, the energy gap amplifies to 2.84 eV. Similarly, at an 8% NiO doping ratio, the energy gap is measured at 2.93 eV.

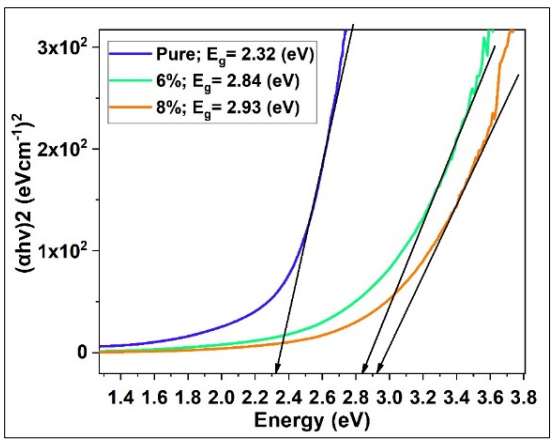

Figure 9. illustrates the variation in the energy gap for the allowed direct transition as a function of photon energy.

3.5- Electrical properties
Continuous conductivity calculation (DC)

By utilizing Equation (6) based on Equation (5), the temperature-dependent electrical conductivity $\sigma_{d.c}$ was determined in the temperature range of 313K-373K. It was observed in (Figure 10.a) that, for a single sample, the electrical resistivity of all the prepared membranes exhibits an inverse relationship with increasing temperature, which is a characteristic behavior of semiconductors. In contrast to conductors, semiconductors exhibit a negative temperature coefficient of resistivity, indicating that the electrical conductivity increases with rising temperature across all membranes. Furthermore, (Figure 10.b) also notes that an increase in the nickel oxide NiO doping ratio is accompanied by a corresponding increase in electrical resistivity, resulting in a decline in electrical conductivity. This decline can be explained as a result of the formation of trap levels near the conduction band's energy gap, leading to an augmentation in defect concentrations within the membrane. The heightened concentration of defects subsequently raises the energy barriers that charge carriers (electrons) must overcome during the conduction process [35]. These findings are consistent with measurements of optical properties, crystal structure distortion, and XRD. The widening of the energy gap arises from a decrease in the abundance of majority charge carriers (electrons) and the emergence of new energy states within the band gaps. Consequently, this decrease leads to diminished electrical conductivity as the nickel oxide doping ratio increases, accompanied by an elevated energy gap value in the doped membrane, as confirmed through energy gap measurements. Consequently, the space for electron mobility expands, necessitating electrons to possess greater energy to transition to the conduction band. Additionally, there is a decrease in the concentration of charge carriers [36,37].

In the evaluation of all membranes, we subtracted the energy level of the Fermi level E_F from the energy level of the conduction band Ec, hence the activation energy Ea was computed.

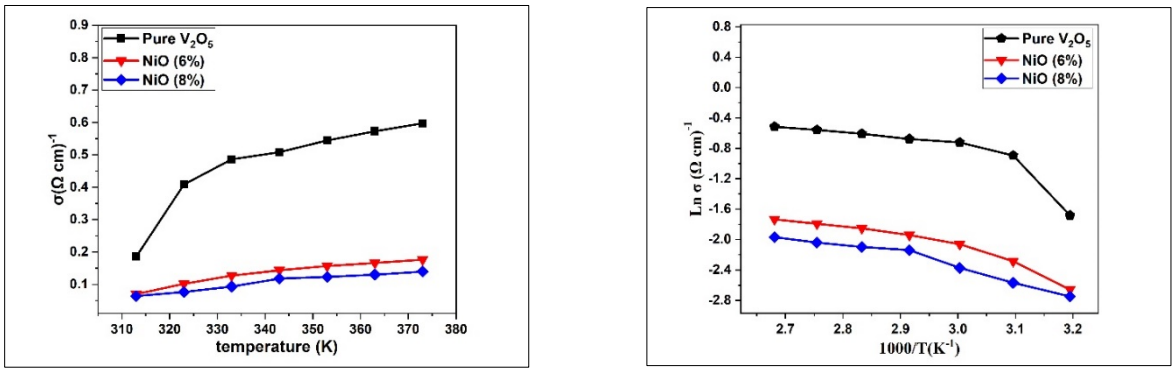

Figure 10. a – Continuous Conductivity ($\sigma_{d.c}$) as a function of temperature change for pure and doped membranes
b - Continuous Conductivity (Ln $\sigma_{d.c}$) as a function of temperature change (1000/T) for pure and doped membranes.

The thin membranes that were prepared possess two distinct activation energy values. The first activation energy is observable within the lower temperature range 313K-343K, characterized by conduction through a hopping mechanism where charge carriers energetically leap from one neutral atom to another within the same energy level in the energy gap. This hopping process takes place within confined energy levels amidst the energy gap, predominantly occurring at grain boundaries, where charge carriers lack the necessary energy to overcome voltage barriers. Consequently, conduction transpires by exciting charge carriers in localized states present within the forbidden energy gap, facilitated by phonons. (Table 2) provides a visual representation, specifying the corresponding temperature intervals for each activation energy. The existence of two activation energies aligns with the XRD examinations conducted on all membranes and the electrical conductivity mechanisms found in polycrystalline semiconducting materials. Regarding the second activation energy E_{a2} or the alternative conduction mechanism, which was computed within the temperature range of 343K-373K, electronic transitions occur due to either thermal excitation or thermionic emission. At elevated temperatures, carriers possess sufficient energy to surmount the voltage barriers arising from grain boundaries and increased potential energy barriers, thereby transitioning into extended states situated above the electron conduction levels Ec. Consequently, grains, grain boundaries, and energy barriers play a pivotal role in determining the electrical characteristics of polycrystalline materials [35,38]. These findings are consistent with the XRD analysis, which demonstrates that the activation energy exhibits an increase alongside the augmentation of the nickel oxide doping ratio. In simpler terms, as the doping ratio rises, the excitation energy required for electrons to reach the conduction band also escalates. These outcomes find support in prior investigations [38]. Within (Table 2), one can find the values denoting direct current conductivity $\sigma_{d.c}$ and activation energy E_a.

Table 2. Continuous Conductivity and Activation Energy Values for Pure and Doped Membranes

Sample	ρ(Ωcm)	$(\sigma_{d.c})_{RT}$ $(\Omega.cm)^{-1}$	$E_{a1}\times10^{-4}$(eV) at Range (313-343)K	$E_{a2}\times10^{-4}$ (eV) at Range (343-373)K
Pure V_2O_5	2.44	0.472	0.434	0.592
V_2O_5+NiO(6%)	8,139	0.135	3.21	2.68
V_2O_5+NiO(8%)	10.13	0.106	4.97	3.65

CONCLUSIONS

In light of the research conducted, it is evident that the polycrystalline nature of all membranes is revealed through X-ray diffraction (XRD) analysis, wherein the size of crystallites diminishes as doping levels rise. By employing field-emission scanning electron microscopy (FE-SEM), the impact of doping on the nanostructure of vanadium oxide is observed, resulting in the transformation from nanotubes to nanosized particles and a subsequent reduction in particle size. This transformation has consequential effects on the optical properties, leading to an escalation in the value of the energy gap. To affirm the reliability and purity of the findings, energy-dispersive X-ray spectroscopy (EDX) yields conclusive and uncontaminated results. Pertaining to the electrical properties, it is noted that the membrane's resistance exhibits an increment with fluctuations in temperature, whereas conductivity experiences a decline as the first activation energy at low temperatures and the second activation energy at high temperatures increase. As a result, these findings hold promise for the development of thermoelectric generators, facilitating the capture and conversion of heat energy into electrical power.

ORCID

Sadon Hassan Hamad, https://orcid.org/0009-0002-9160-7256; **Huda Saadi Ali,** https://orcid.org/0000-0003-4115-3591

REFERENCES

[1] H.M.R. Giannetta, C. Calaza, D.G. Lamas, L. Fonseca, and L. Fraigi, "Electrical transport properties of V_2O_5 thin films obtained by thermal annealing of layers grown by RF magnetron sputtering at room temperature," Thin Solid Films, **589**, 730-734 (2015). https://doi.org/10.1016/j.tsf.2015.06.048

[2] Z. Zheng et al., "The Optical Properties of V_2O_5 Films Deposited on Single Crystal Diamond Under Homogenizing Preparation Technology," Integrated Ferroelectrics, **235**(1), 100-105 (2023). https://doi.org/10.1080/10584587.2023.2192674

[3] S. Senapati, and S. Panda, "Effect of aging of V_2O_5 sol on properties of nanoscale films," Thin Solid Films, **599**, 42-48 (2016). https://doi.org/10.1016/j.tsf.2015.12.045

[4] B. Priya, P. J. Arunima, and T. Kumar, "Structural, morphological and optical properties of V2O5 thin films for," Growth And Characterization Of Semiconductor Nanostructure For Device Applications, p. 106, 2023.

[5] J. Huotari, J. Lappalainen, J. Eriksson, R. Bjorklund, E. Heinonen, I. Miinalainen, J. Puustinen, et al., "Synthesis of nanostructured solid-state phases of V_7O_{16} and V_2O_5 compounds for ppb-level detection of ammonia," Journal of Alloys and Compounds, **675**, 433-440 (2016). https://doi.org/10.1016/j.jallcom.2016.03.116

[6] R. Moskalyk, and A.M. Alfantazi, "Processing of vanadium: a review," Minerals Engineering, **16**(9), 793-805 (2003). https://doi.org/10.1016/S0892-6875(03)00213-9

[7] H. Khmissi, S.A. Mahmoud, and A.A. Akl, "Investigation of thermal annealing effect on the microstructure, morphology, linear and non-linear optical properties of spray deposited nanosized V_2O_5 thin films," Optik, **227**, 165979 (2021). https://doi.org/10.1016/j.ijleo.2020.165979

[8] Y. Yue, L. Ma, J. Sun, H.-K. Jeong, and H. Liang, "Super-hierarchical Ni/porous-Ni/ V_2O_5 nanocomposites," RSC Adv. **7**(64), 40383-40391 (2017). https://doi.org/10.1039/C7RA06446B

[9] S.F. Cogan, N.M. Nguyen, S.J. Perrotti, and R.D. Rauh, "Optical properties of electrochromic vanadium pentoxide," Journal of Applied Physics, **66**(3), 1333-1337 (1989). https://doi.org/10.1063/1.344432

[10] K. Schneider, "Optical properties and electronic structure of V_2O_5, V_2O_3 and VO_2," Journal of Materials Science: Materials in Electronics, **31**(13), 10478-10488 (2020). https://doi.org/10.1007/s10854-020-03596-0

[11] V.S. Vijay, R. Varghese, A. Sakunthala, S. Rajesh, and B.J.V. Vidhya, "Highly crystalline V_2O_5 and V_6O_{13} thin films by PLD and a study on morphology transition of V_2O_5 by post annealing," Vacuum, **187**, 110097 (2021). https://doi.org/10.1016/j.vacuum.2021.110097

[12] M. Zou, "Deposition Methods and Thermoresistive Properties of Vanadium Oxide and Amorphous Silicon Thin Films," M.Sc. Thesis, University of Dayton, 2015. http://rave.ohiolink.edu/etdc/view?acc_num=dayton1446477859

[13] H. Lv, X. Tian, M.Y. Wang, and D. Li, "Vibration energy harvesting using a phononic crystal with point defect states," Appl. Phys. Lett. **102**(3), 034103 (2013). https://doi.org/10.1063/1.4788810

[14] M. Bonomo, "Synthesis and characterization of NiO nanostructures: a review," Journal of Nanoparticle Research, **20**(8), 222 (2018). https://doi.org/10.1007/s11051-018-4327-y

[15] H. Xuemei, S. Yukun, and B. Bai, "Fabrication of cubic pn heterojunction-like NiO/In V_2O_3 composite microparticles and their enhanced gas sensing characteristics," Journal of Nanomaterials, **2016**, 7589028 (2016). https://doi.org/10.1155/2016/7589028

[16] A.N. Mohsin, B.H. Adil, H.Q. Khaleel, R.A. Al-Ansari, and I.R. Swadi, "Non-Thermal Plasma Effect Of Li Doped Nio Thin Films Prepared By The Spray Pyrolysis Technique For Sensor Applications," International Journal of Applied Sciences and Technology, **4**(1), 80-97 (2022). http://dx.doi.org/10.47832/2717-8234.10.8

[17] A.S. Fathima, I.K. Punithavthy, A. Rajeshwari, A. Sindhya, and A. Muthuvel, "Structural, Optical and Electrical Properties of V_2O_5 Thin films at different Molarities by Spray pyrolysis method," Journal of the Nigerian Society of Physical Sciences, **4**(4), 1050 (2022). https://doi.org/10.46481/jnsps.2022.1050

[18] B. Priya, P. Jasrotia, I. Sulania, D.K. Chaudhary, R. Gupta, A.S. Verma, R. Kumar, *et al*., "Tuning of Structural and Morphological Characteristics of V_2O_5 Thin Films Using Low Energy 16 keV N+ for Optical and Wetting Applications," ECS Advances, **2**(2), 021002 (2023). https://doi.org/10.1149/2754-2734/accafc

[19] Y.S. Thakur, A.D. Acharya, and S. Sharma, and Bhawna, "Reinforcement of V_2O_5 nanoparticle in polyaniline to improve the optical and UV-shielding properties," Results in Optics, **11**, 100400 (2023). https://doi.org/10.1016/j.rio.2023.100400

[20] R. Ramadan, M. Ahmed, and M.M. El-Masry, "PVDF-based $(V_2O_5)_x(Mn_{0.4}Fe_{2.6}O_4)_{(2-x)}$, x=[0.2, 0.4, 0.6, 0.8, and 1] nanocomposites for tailoring the optical and nonlinear optical properties of PVDF," Polym. Bull. 1436-2449 (2023). https://doi.org/10.1007/s00289-023-04850-1

[21] M. Abdelrazek, A.E. Hannora, R.M. Kamel, I. Morad, M.J.O. El-Desoky, and Q. Electronics, "Effect of lanthanum doping on the structure and optical properties of nanocrystalline vanadium pentoxide films prepared by sol-gel method," **55**(6), 491 (2023). https://doi.org/10.21203/rs.3.rs-2461694/v1

[22] Y. Xia, C. Calahoo, B. P. Rodrigues, K. Griebenow, L. Graewe, and L. Wondraczek, "Structure and properties of cerium phosphate and silicophosphate glasses," Journal of the American Ceramic Society, **106**(5), 2808-2819 (2023). https://doi.org/10.1111/jace.18936
[23] N. Komal, M. A. Mansoor, M. Mazhar, M. Sohail, Z. Malik, and M. Anis-ur-Rehman, "Effect of (Sm, In) Doping on the Electrical and Thermal Properties of Sb_2Te_3 Microstructures," ACS Omega, **8**(11), 9797-9806 (2023). https://doi.org/10.1021/acsomega.2c05859
[24] N. Bhardwaj, and S. Mohapatra, "Structural, optical and gas sensing properties of Ag-SnO_2 plasmonic nanocomposite thin films," Ceramics International, **42**(15), 17237-17242 (2016). https://doi.org/10.1016/j.ceramint.2016.08.017
[25] R.K. Jain and A. Khanna, "Structural, optical and electrical properties of crystalline V_2O_5 films deposited by thermal evaporation and effects of temperature on UV–vis and Raman spectra," Optik, **144**, 271-280 (2017). https://doi.org/10.1016/j.ijleo.2017.06.104
[26] Y.Z. Zheng, H. Ding, E. Uchaker, X. Tao, J.F. Chen, Q. Zhang, and G. Cao, "Nickel-mediated polyol synthesis of hierarchical V_2O_5 hollow microspheres with enhanced lithium storage properties," J. Mater. Chem. A, **3**(5), 1979-1985 (2015). https://doi.org/10.1039/C4TA05500D
[27] P. Hu, P. Hu, T.D. Vu, M. Li, S. Wang, Y. Ke, X. Zeng, et al., "Vanadium Oxide: Phase Diagrams, Structures, Synthesis, and Applications," Chem. Rev. **123**(8), 4353-4415 (2023). https://doi.org/10.1021/acs.chemrev.2c00546
[28] T.K. Le, M. Kang, V.T. Tran, and S.W. Kim, "Relation of photoluminescence and sunlight photocatalytic activities of pure V_2O_5 nanohollows and V_2O_5/RGO nanocomposites," Materials Science in Semiconductor Processing, Materials Science in Semiconductor Processing, **100**, 159-166 (2019). https://doi.org/10.1016/j.mssp.2019.04.047
[29] T.K. Le, M. Kang, and S.W. Kim, "Room-temperature photoluminescence behavior of α-V2O5 and mixed α-β phase V_2O_5 films grown by electrodeposition," Materials Science in Semiconductor Processing, **94**, 15-21 (2019). https://doi.org/10.1016/j.mssp.2019.01.026
[30] Y. Vijayakumar, P. Nagaraju, T. Sreekanth, U. Rushidhar, P.S. Reddy, "Effect of precursor volume on chemically sprayed V_2O_5 thin films for acetaldehyde detection," Superlattices and Microstructures, **153**, 106870 (2021). https://doi.org/10.1016/j.spmi.2021.106870
[31] H. Liu, X. Liang, T. Jiang, Y. Zhang, S. Liu, X. Wang, X. Fan, *et al*., "Analysis of structural morphological changes from 3DOM V_2O_5 film to V_2O_5 nanorods film and its application in electrochromic device," **238**, 111627 (2022). https://doi.org/10.1016/j.solmat.2022.111627
[32] P. Deepika, H. Vinusha, B. Muneera, N. Rekha, and K. S. Prasad, "Vanadium oxide nanorods as DNA cleaving and anti-angiogenic agent: novel green synthetic approach using leaf extract of Tinospora cordifolia," Current Research in Green and Sustainable Chemistry, vol. 1, pp. 14-19, 2020. https://doi.org/10.1016/j.crgsc.2020.04.001
[33] C.K.P. Neeli, V.S.P. Ganjala, V. Vakati, K. Seetha, R. Rao, and D R. Burri, "V_2O_5/SBA-15 nanocatalysts for the selective synthesis of 2,3,5-trimethyl-1, 4-benzoquinone at room temperature," New J. Chem. **40**(1), 679-686 (2016). https://doi.org/10.1039/C5NJ02399H
[34] M. Thirumoorthi, and J.T.J. Prakash, "A study of Tin doping effects on physical properties of CdO thin films prepared by sol–gel spin coating method," Journal of Asian Ceramic Societies, **4**(1), 39-45 (2016). https://doi.org/10.1016/j.jascer.2015.11.001
[35] L.K. Emhjellen, X. Liu, J.M. Polfus, and R. Haugsrud, "Native point defects and polaron transport in zirconium pyrovanadate," Solid State Ionics, **386**, 116033 (2022). https://doi.org/10.1016/j.ssi.2022.116033
[36] A. Qasrawi, N.M. Gasanly, "Temperature effect on dark electrical conductivity, Hall coefficient, space charge limited current and photoconductivity of $TlGaS_2$ single crystals," Semiconductor Science and Technology, **20**(5), 446 (2005). https://doi.org/10.1088/0268-1242/20/5/021
[37] S.K. Sinha, "Effect of temperature on structural, optical and electrical properties of pulsed-laser deposited W-doped V_2O_5 thin films," Superlattices and Microstructures, **125**, 88-94 (2019). https://doi.org/10.1016/j.spmi.2018.10.029
[38] Z. Zhang, C. Yin, L. Yang, J. Jiang, Y. Guo, "Optimizing the gas sensing characteristics of Co-doped SnO_2 thin film based hydrogen sensor," Journal of Alloys and Compounds, **785**, 819-825 (2019). https://doi.org/10.1016/j.jallcom.2019.01.244

ВПЛИВ ЛЕГУВАННЯ НА ЕЛЕКТРОПРОВІДНІСТЬ ПЛІВОК ОКСИДУ ВАНАДІЮ (V_2O_5), ЛЕГОВАНИХ ОКСИДОМ НІКЕЛЮ (NiO) ПІДГОТОВЛЕНИХ ІМПУЛЬСНИМ ЛАЗЕРНИМ ОСАДЖЕННЯМ (ІЛО)

Садон Хасан Хамад, Худа Сааді Алі
Факультет фізики, Освітній коледж чистих наук, Університет Тікріту, Салагуддін, Ірак

У цьому дослідженні основна увага була зосереджена на дослідженні тонких плівок оксиду ванадію (скорочено V_2O_5) з різними рівнями легування оксидом нікелю (NiO) (X = 0, 6, 8)%. Плівки були створені методом імпульсного лазерного осадження (PLD). Тонкі плівки виготовляли та піддавали відпалу при 450°C протягом однієї години. Структурні властивості плівок досліджували за допомогою дифракційного методу XRD, за допомогою якого було виявлено, що склад плівок є полікристалічним, що має орторомбічну структуру. Примітно, що плівки показали помітне вирівнювання вздовж площини (111), що проявляється під кутом приблизно 27,889˚. Технологія FE-SEM була використана для дослідження та оцінки морфології поверхні тонких плівок. Це показало трансформацію форми нанотрубки в сферичну. Після застосування рентгенівського методу EDX було визначено, що плівки містять елементарні компоненти ванадію (V), нікелю (Ni) і кисню (O), що відповідає співвідношенням легування. Оцінку оптичних властивостей плівок проводили за допомогою УФ-видимого спектрофотометра, який продемонстрував зниження абсорбції та коефіцієнта поглинання, а також збільшення енергетичної забороненої зони з 2,32 еВ до 2,93 еВ. Результати електричної провідності вказують на зменшення провідності постійного струму (σd.c) зі збільшенням коефіцієнта легування, тоді як енергія активації (Ea) зростає. Отже, ці плівки можуть бути використані в термоелектричних генераторах.

Ключові слова: *тонкі плівки; оксид ванадію (V_2O_5); імпульсне лазерне осадження (PLD); відпал; електричні властивості*